AIAA JOURNAL
Vol. 43, No. 10, October 2005

Investigation of Delamination Caused by Impact by Using a Cohesive-Layer Model

Yupeng Li* and Srinivasan Sridharan†
Washington University in St. Louis, St. Louis, Missouri 63130

A numerical simulation of crack growths in specimens tested under static loading and low-velocity impact is undertaken using a cohesive-layer model. The basis on which the model is constructed and the identification of critical strain-energy release rates from available experimental results of load vs crack length relationship are described. The model is then used to trace the crack growth for given initial crack lengths. It is demonstrated that in a strict sense there is no unique relationship between the load and crack length because of the nonlinearities involved, a factor that accounts for the scatter in the experimental results. The relationship between crack growth under static loading and dynamic load application associated with impact is studied in some detail for the test specimens. In general the cracks are seen to grow to greater lengths under dynamic loading than under static loading. Once again the initial crack length is seen to be a significant factor in the total crack length reached under a given dynamic load. The results demonstrate that a program of a series of successive impacts with steadily increasing amplitudes results in higher delamination than that caused by the direct application of the impact loading with the highest amplitude in the series.

Nomenclature

E_1, E_2	=	longitudinal and transverse Young's moduli, respectively
G_I	=	modal I component (opening mode) of strain-energy release rate
G_{II}	=	modal II component (shear mode) of strain-energy release rate
G_{I_c}	=	mode I critical strain-energy release rate
G_{II_c}	=	mode II critical strain-energy release rate
G_{total}	=	total strain-energy release rate
G_{12}	=	shear modulus
h	=	overall thickness of the specimen
h_c	=	current thickness of cohesive layer
h_0	=	initial thickness of cohesive layer
l_{cr}	=	current crack length related with given external load P
$l_{\max}$	=	maximum crack growth for a given $P_{\max}$
l_0	=	initial crack length
P	=	external load
P_{l_0}	=	load at which the crack growth just initiates
$P_{\max}$	=	amplitude of impact load vs time relationship
U	=	axial displacement
V	=	lateral displacement
v	=	impact velocity
w	=	width of the specimen
α_1, α_2	=	longitudinal and transverse thermal expansion coefficients, respectively
ΔT	=	change in temperature
$\Delta\varepsilon_n, \Delta\gamma$	=	increments of normal strain and shear strain, respectively
ν_{12}	=	Poisson's ratio
$\sigma_{\max}, \tau_{\max}$	=	transverse and shear strengths of cohesive layer, respectively
σ_n, τ	=	current normal and shearing stresses, respectively

Received 22 April 2004; revision received 28 January 2005; accepted for publication 20 February 2005.

*Research Assistant, Boeing Fellow, Department of Civil Engineering.
†Professor, Campus Box 1130, Department of Civil Engineering, 1 Brookings Drive; ssrid@seas.wustl.edu. Senior Member AIAA.

Introduction

COMPOSITE laminates subjected to foreign object impact can sustain severe damage, which might be internal and not always visible on the surface. The damage can take the form of matrix cracking and delamination. The latter form of damage can lead to significant reduction in the compressive strength of the laminate.

The literature on the damage caused by impact is vast, and the topic is of considerable practical interest. The developments in the field up to 1998 have been summarized by Abrate.[1] There are several independent variables, such as impactor mass, impact velocity, contact area, and properties of the laminate, that govern the dynamic response and the extent of damage in the laminate. In this paper, attention is focused on the low-velocity impact scenario, where the mass of the impactor is considerably greater than that of the target, the contact time is considerably longer than the fundamental time period of oscillation of the laminate, and the impact velocity is considerably smaller than characteristic wave propagation speeds. It has been suggested by Jih and Sun[2] that under these conditions a quasi-static analysis is often sufficient to study the growth of delamination.

An elegant approach to study the initiation and growth of delamination is the cohesive-layer model. The opening of the crack is described in terms of a nonlinear traction vs relative displacement relationship or alternately stress-strain relations, which include a significant softening phase. The basic concept was proposed by Barrenblatt[3] and Dugdale,[4] but their implementations were highly simplified. Further refinements and applications are from, among others, Williams,[5] Schapery,[6] and Ungsuwarungsri and Knauss.[7] Extensive analyses of void nucleation and void coalescence have been performed by Needleman[8,9] and his associates using cohesive-layer models. More recently variants of the model have been proposed by Shahwan and Waas,[10] Song and Waas,[11] Rahulkumar et al.,[12] and El-Sayed and Sridharan.[13,14] Computational issues of the cohesive-layer model have been investigated extensively by Alfano and Crisfield.[15]

The present authors prefer to use a physically based cohesive-layer model having strengths and initial stiffness that are characteristic of the medium in which the delamination crack runs; further, a stress-strain relationship rather than a traction-relative displacement relationship is postulated for the material. Here the stress is "true" stress corotational with the local axes of the cohesive-layer element, and the strain increments are based on the current geometry and therefore close to logarithmic or "true" strains. This has the advantage of being able to handle large rotations and therefore comes in handy in analyses with significant geometric nonlinearities.

A question of pivotal importance in the use of the cohesive-layer model is the selection of its properties and the allied issue of the crack growth criterion. Evidently, in two-dimensional problems, the critical values of the modal components (G_{I_c}, opening mode; G_{II_c}, shear mode) of the strain-energy release rates (SERR) are the most important parameters and these are supposed to be known. Considering mode I for example, there are four more parameters, that is to say, initial stiffness, maximum strength, thickness of the cohesive layer, and the maximum strain needed to be determined. It has been shown[14] that if the initial stiffness and maximum strength are chosen so as to reflect the actual material through which the crack runs, and the other two parameters are determined from the assumed shape of the stress-strain curve and the energy release rate, the model gives satisfactory results and is insensitive to small changes in stiffness and maximum strength. Blackman et al.[16] and Alfano and Crisfield[15] have considered wide variations in the maximum strength and come to similar conclusions.

There are occasions, however, where the critical values of SERR are not known and what is available is a set of loads P and the corresponding crack lengths l_{cr} as determined from tests. In this case, one can attempt to determine G_{I_c} and G_{II_c} by finding G_I and G_{II} by the virtual crack closure technique (VCCT) and fitting them into an assumed crack growth criterion. Again, this procedure might fail to yield reasonable values of G_{I_c} and G_{II_c}. Although there might be several reasons why this can happen, one fundamental fact remains: the elastic values of G_I and G_{II} in bimaterial fracture as determined by VCCT do not converge.

The case in point is the experimental results produced by Jih[17] and reported in a shortened form by Jih and Sun.[2] Two typical test configurations made up of carbon epoxy were fabricated and tested under both quasi-static loading and low-velocity impact. These are illustrated in Figs. 1a and 1b. The primary objective of these tests was to investigate the effect of transverse flexural cracking on delamination growth. It is seen that the chosen configurations incorporate discontinuities that mimic transverse cracks. An initial delamination of unspecified length is introduced during fabrication in each case. The results are available in the form of plots of P (transverse load) vs l_{cr} (the crack length). The results show some scatter, and the scatter band is indicated in Figs. 2a and 2b. Using this information, the G_I and G_{II} values are computed using VCCT for various crack lengths in the present work. It will be shown that it is impossible to postulate any meaningful interaction criterion $F(G_I/G_{I_c}, G_{II}/G_{II_c}) = 0$ that is consistent with the experimental results.

Jih and Sun do not employ an interactive criterion in their crack-growth analysis. They tried to explain the crack growth using a criterion based on the total SERR, that is, $G_{\text{total}} > G_c$. With this criterion the experimental and theoretical load vs crack length relationships show a discrepancy of 20% in some cases. The present work revisits these experimental results and seeks to explain the same in terms of a cohesive-layer model.

Because the cohesive-layer model is selected as the tool for tracing the crack growth, it is at once consistent and expedient to determine the values of G_{I_c} and G_{II_c} using the same tool. Thus the cohesive-layer model performs in the present work a dual function of identifying the critical values of SERR and tracing the crack growth as well. Both static and dynamic delamination initiation and growth problems are considered.

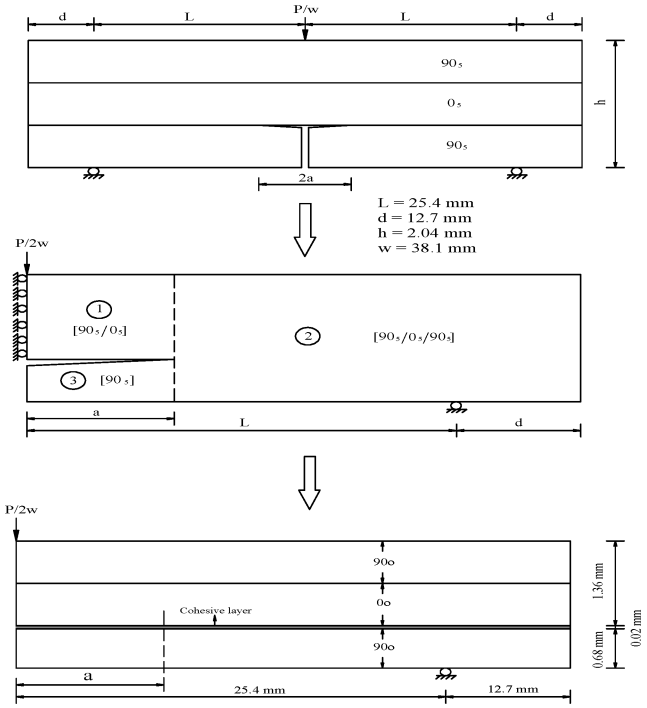

a) Test configuration 1

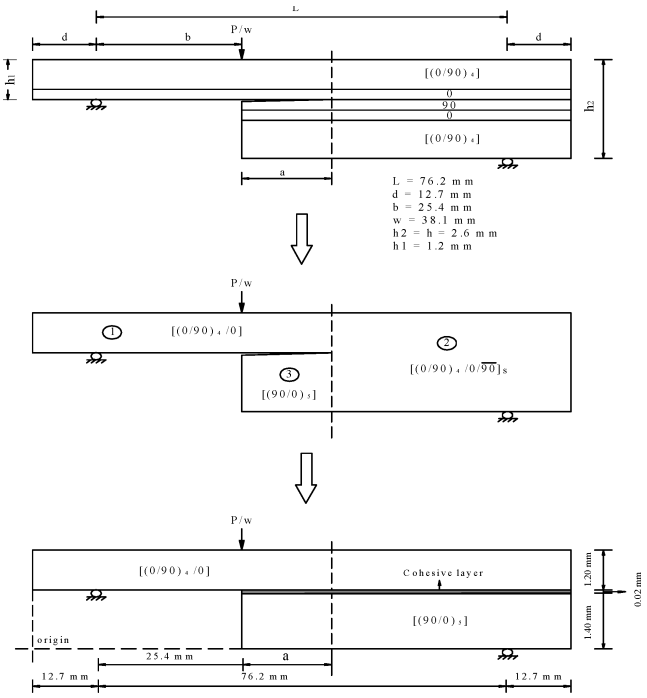

b) Test configuration 2

Fig. 1 Configuration of test specimens.

Parameter Identification from Test Results

Test Configurations

Figures 1a and 1b show two test configurations designated as TC-1 and TC-2, respectively. The full details of the tests are reported by Jih,[17] and the necessary details are given in this paper for the sake of completeness. Shown in Figs. 1a and 1b are laminated beam specimens whose widths ($w = 38.1$ mm) are of the same order of magnitude as the span, subjected to a line load of magnitude P, that is, of intensity P/w per unit width. The material of the specimens is AS4/3501-6 graphite/epoxy. The following material properties are given by Jih[17]:

$$E_1 = 139\ \text{GPa}, \qquad E_2 = 9.86\ \text{GPa}, \qquad G_{12} = 5.24\ \text{GPa}$$
$$\nu_{12} = 0.3, \qquad \alpha_1 = -0.54\ \mu\varepsilon/^\circ\text{C}, \qquad \alpha_2 = 27.2\ \mu\varepsilon/^\circ\text{C}$$

Temperature drop from curing condition was reported as $\Delta T = -156^\circ$C. The effects of curing stresses are important[2] and are duly considered in the present study.

TC-1 (Fig. 1a) consists of three sublaminates, the outer ones being composed of five plies with fibers running in the transverse direction (90-deg plies), and the interior one has fibers running in the longitudinal direction of the beam (0-deg plies). The bottom ply is cut right at the middle and a preimplanted delamination of certain length $2a$ is installed between the bottom 90 deg and the next 0-deg sublaminates during fabrication. Because of the symmetry of

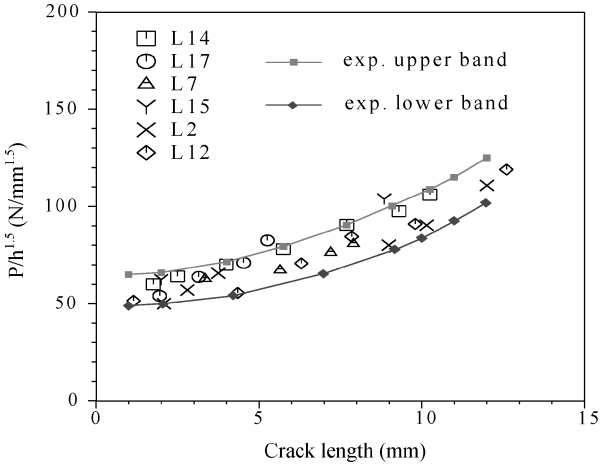

a) Test configuration 1

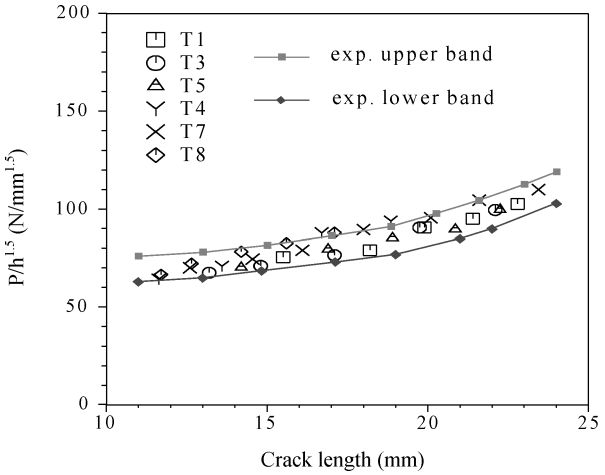

b) Test configuration 2

Fig. 2 Experimental transverse load vs crack length relationship.

the configuration, it is sufficient to deal with one-half of the beam carrying a load of $p = P/2w$ per unit width.

TC-2 (Fig. 1b) is designed to be significantly asymmetric, ostensibly with the objective of making it distinctly different from TC-1. It is built of an upper sublaminate with a ply sequence of $[(0/90)_4/0]$ of length 101.6 mm and a lower sublaminate with a ply sequence of $[(90/0)_5]$ of length 63.5 mm. A preimplanted delamination of certain length a is installed between these sublaminates. The loading arrangement and other details of the setup are given in Fig. 1b.

Load vs Crack Length Relationship

During the tests, specimens were loaded in steps and unloaded to measure crack extensions. Thus Jih and Sun were able to associate a given crack length with a certain load and an increase in crack length was possible only under the increase of load. Thus the crack growth occurred under stable conditions. The transverse load P and the corresponding crack length l_{cr} relationships are given in Figs. 2a and 2b for TC-1 and TC-2, respectively. The results show some significant scatter.

Use of VCCT as a Tool of Parameter Identification

To study the growth of delamination in the test specimens under investigation as well as to be able to transport the results to other laminates fabricated out of the same material, it is necessary to develop a crack-growth criterion. Such a criterion is generally based on the critical values of SERR in the two modes, that is, G_{I_c} and G_{II_c}. To develop such a criterion, the magnitudes of G_I and G_{II} are computed for given crack lengths using the corresponding loads. Two typical sets of values of P and l_{cr} are selected from each test configuration, and the corresponding points are indicated in Figs. 2a and 2b. The values of values of G_I and G_{II} obtained using linear elastic VCCT in each of the four cases are given in Tables 1 and 2. The results indicate that both the values of the individual components as well as the total SERR increase with crack length in each test configuration and also from TC1 to TC2. This makes it impossible to extract the critical values G_{I_c} and G_{II_c} using any meaningful crack-growth criterion. A further attempt was made to remedy the situation by accounting for geometric nonlinearities and correcting the effects of local rotation at the crack tip in the determination of G_I and G_{II}. However such a calculation still did not lead to a satisfactory resolution of G_{I_c} and G_{II_c}.

Table 1 G_I and G_{II} from VCCT for TC-1

Load, N/mm$^{1.5}$: $P/h^{1.5}$	Load, N/mm: $p = P/2w$	Crack length l_{cr}, mm	G_I, N/m	G_{II}, N/m
57	2.18	1.92	182	87
102	3.90	11.12	198	95

Table 2 G_I and G_{II} from VCCT for TC-2

Load, N/mm$^{1.5}$: $P/h^{1.5}$	Load, N/mm: $p = P/w$	Crack length l_{cr}, mm	G_I, N/m	G_{II}, N/m
71	7.81	12.72	206	88
105	11.55	23.4	224	97

One of the issues in the foregoing approach is the applicability of linear elastic analysis, which implies that a given crack length corresponds to a certain load. This approach is based on the assumption of small deflections and the consequent uniqueness of the solution. However, when the effects of geometric nonlinearities and the history of energy dissipation during crack growth become significant, one can have differing values of P for a certain crack length depending upon the initial crack length. This point is discussed further in one of the later sections of the paper.

Construction of Cohesive-Layer Model

In an attempt to overcome this impasse, authors investigated the possible use of a cohesive-layer model. This is a layer of fictitious material inserted between the planes liable to separate. The principal function of the cohesive-layer model is to trace the growth of delaminations. This is done on the basis of the modal components of strain-energy release rates, which are computed from the normal and shearing stress and strain components prevailing in the cohesive layer. It is therefore natural to turn to this model for obtaining the critical values of the components of SERR that are in accord with experimentally recorded values of P and the crack length l_{cr}.

The cohesive-layer model is characterized by a small number of parameters that must be appropriately selected. Of these, the thickness of this layer h_0 is based on the observed dimensions of the process zone of composite materials,[18] that is, $h_0 = 0.02$ mm. This dimension then plays the role of the length scale in the study. The cohesive layer consists of four node elements $h_0 \times h_0$ (aspect ratio $= 1$). The transverse modulus E_2 is the same as that of the composite material. The other properties, that is, E_1 and G_{12} (longitudinal and shear moduli), α_1, α_2 (coefficients of thermal expansion in the longitudinal and transverse directions) are all taken as the weighted averages of the respective values of the layers above and below the delamination plane. The transverse and shear strengths of the cohesive-layer material are those of the graphite epoxy and are taken as 41 MPa ($\sigma_{\max}$) and 97 MPa ($\tau_{\max}$), respectively.[19] Insofar as G_{I_c} and G_{II_c} are not known, the maximum strain (normal and shear) cannot be determined a priori, and therefore the stress-strain response of the cohesive layer, and in particular its softening phase, cannot be postulated. An elastic perfectly plastic response is therefore assumed.

The cohesive material response calculations are performed in a module (UMAT) attached to a general-purpose nonlinear finite element program (Abaqus[20]). The stresses and strains of the cohesive-layer element are referred to axes that rotate with the element. Thus the effect of rigid-body rotations is eliminated in the incremental

strain-displacement relations. The incremental strains are based on the current dimensions, and so the total strain is approximately logarithmic (vide *Abaqus Theory Manual*[21]). As the nonlinear analysis proceeds, the values of G_I and G_{II} are computed by summation over a large number of small increments as follows:

$$G_I = \sum \sigma_n h_c \, \Delta\varepsilon_n, \qquad G_{II} = \sum \tau h_c \, \Delta\gamma \tag{1}$$

The values of G_I and G_{II} corresponding to the load at incipient crack growth must satisfy a crack-growth criterion.

Abaqus Model

The nonlinear finite element analyses are conducted using Abaqus[20] incorporating a user supplied material subroutine (UMAT) for the cohesive layer. Plane-strain elements were employed throughout. The cohesive layer and its immediate surroundings were modeled using four-noded elements with reduced integration (CPE4R) with aspect ratio of unity or close to unity. However Poisson's effect in the cohesive-layer elements is neglected. Elsewhere eight-noded elements (CPE8R) were employed in the interests of robustness. As already mentioned, the size of the cohesive-layer elements was 0.02 mm square. The mesh generated was verified to be sufficiently accurate for crack initiation and growth simulations.

Determination of G_{I_c} and G_{II_c}

The following procedure is employed for the determination of the critical values of G_I and G_{II}. First, a certain crack length is chosen for each test configuration. This is chosen to be close to the length of preimplanted delamination, that is, the shortest one for which the test data of P are available. A short crack length is preferred, as at the beginning of loading, the crack surfaces are expected to be smooth and free of localized "bumps." A thermal stress analysis is first performed to compute the curing stresses as they do influence the results, especially for TC-1.

Nonlinear analyses are now run for TC-1 and TC-2, each for the selected crack length, and the values of G_I and G_{II} as given by the cohesive-layer model were obtained for values of P covering the core of the scatter band. Thus five sets of P, G_I, and G_{II} values are obtained for each case (Tables 3 and 4). The table also gives values of G_{total} (SERR) as obtained from nonlinear elastic analyses.

From an inspection of Tables 3 and 4, it is clear that G_I and G_{II} as determined from the cohesive-layer model do not sum up to G_{total} as determined from nonlinear elastic analysis without the cohesive layer. The discrepancy is particularly noticeable for TC-2. Insofar as G_{total} is a global parameter calculable from prescribed loads working through corresponding deflections, it is of some concern that G_I and G_{II} computed from cohesive-layer models do not add up to this value. However, the very introduction of the cohesive layer slightly alters the structural configuration. Further, the plasticity is not really localized near the crack tip, but several (about 15) elements in the cohesive layer are in the plastic range at incipient crack growth. Hence it appears unrealistic that G_I and G_{II} as found from the cohesive layer should add up to G_{total} of the nonlinear elastic calculation. Because the deflections under the load are not reported, it is not possible to assess the relative accuracies of the total G coming from the two divergent approaches.

Returning to the evaluation of the critical values of G_I and G_{II} each pair of G_I and G_{II} values from TC-1 can be used in conjunction with each of the five pairs of G_I and G_{II} of TC-2 to determine the values of G_{I_c} and G_{II_c}, taking a simple linear interactive criterion for crack growth in the form

$$G_I/G_{I_c} + G_{II}/G_{II_c} = 1 \tag{2}$$

Thus there are results of 25 pairs of G_{I_c} and G_{II_c} values. However, from these one must weed out values in which 1) G_I values of TC1 and TC2 pair are so close that the values of G_{II_c} turn out to be inordinately high (say, >5000 N/m) and 2) G_{II_c} comes out to be smaller than G_{I_c}. The remaining sets of values are shown in Table 5.

An inspection of the values of G_{I_c} and G_{II_c} thus obtained reveals that G_{I_c} varies over a relatively narrow range (from 195 to 242 N/mm), whereas G_{II_c} varies over a much larger range (263 to 2085 N/mm). It is apparent that the problem is dominated by fracture in mode I with mode II playing a relatively minor role. It is this feature that makes it difficult to pin down G_{II_c}. Reasonable estimates of G_{I_c} and G_{II_c} can be obtained by averaging all of the respective values in Table 5. These are found as $G_{I_c} = 216$ N/mm and $G_{II_c} = 620$ N/mm. These appear to be reasonably close to values reported in literature.[18]

Prediction of P vs l_{cr} Relationship for Crack-Growth Initiation

Static nonlinear analyses are run for both TC-1 and TC-2 starting with differing values of crack lengths (with crack tips at one of the four station points A-D; Table 6 and the corresponding loads at incipient crack growth were determined using the criterion in Eq. (2) and the already determined values of G_{I_c} and G_{II_c}. The results are given in Table 6. Mode-mixity remains approximately the same, that is, more or less independent of the initial crack length for each test configuration. The P vs l_{cr} relationships are plotted in Fig. 3 for the two cases. The theoretical predictions lie well within the scatter band of the experimental results.

Table 3 Values of G_I and G_{II} for TC-1 under l_{cr} = 1.92 mm

Case	$P/h^{1.5}$, N/mm$^{1.5}$	$p = P/2w$, N/mm	G_I, N/m	G_{II}, N/m	G_{total} (elastic), N/m
1	54	2.065	186.5	32.9	213.3
2	56	2.141	193.5	34.3	230.7
3	58	2.218	200.7	35.7	248.1
4	60	2.294	208.0	37.1	265.6
5	62	2.371	215.5	38.5	283.0

Table 4 Values of G_I and G_{II} for TC-2 under l_{cr} = 12.72 mm

Case	$P/h^{1.5}$, N/mm$^{1.5}$	$p = P/w$, N/mm	G_I, N/m	G_{II}, N/m	G_{total} (elastic), N/m
1	68	7.48	176.1	48.7	269.8
2	69	7.59	182.0	50.1	276.5
3	70	7.70	188.0	51.6	286.1
4	71	7.81	193.0	53.4	292.3
5	72	7.92	198.8	55.1	298.5

Table 5 G_{I_c} and G_{II_c} from TC-1 and TC-2 results[a]

TC1 case	TC2 case	TC1: G_I, N/m	TC1: G_{II}, N/m	TC2: G_I, N/m	TC2: G_{II}, N/m	G_{I_c}, N/m	G_{II_c}, N/m
1	1	186.5	32.9	176.1	48.7	208.2	316.2
1	2	186.5	32.9	182.0	50.1	195.1	745.7
2	2	193.5	34.3	182.0	50.1	218.5	300.2
2	3	193.5	34.3	188.0	51.6	204.4	642.9
3	3	200.7	35.7	188.0	51.6	229.2	287.0
3	4	200.7	35.7	193.0	53.4	216.2	497.1
3	5	200.7	35.7	198.8	55.1	204.2	2085.0
4	4	208.0	37.1	193.0	53.4	242.1	263.1
4	5	208.0	37.1	198.8	55.1	227.0	444.1

[a]Average G_{I_c} 216 N/m and average G_{II_c} 620 N/m.

Table 6 Loads at incipient crack growth for different crack lengths

Station point	Crack length, mm	$p = P/2w$, N/mm	$P/h^{1.5}$, N/mm$^{1.5}$	G_I, N/m	G_{II}, N/m	$\frac{G_I}{G_{I_c}} + \frac{G_{II}}{G_{II_c}}$
			Test configuration 1			
A	1.92	2.25	58.84	204.2	36.5	1.00
B	4.8	2.58	67.47	204.2	36.6	1.00
C	7.16	2.93	76.63	203.9	36.9	1.00
D	11.12	3.80	99.38	203.1	37.2	1.00
			Test configuration 2			
A	12.72	7.90	71.79	197.1	55.1	1.00
B	16.24	8.74	79.43	197.1	55.8	1.00
C	20.40	10.06	91.42	196.4	56.3	1.00
D	23.40	11.25	102.24	196.3	57.0	1.00

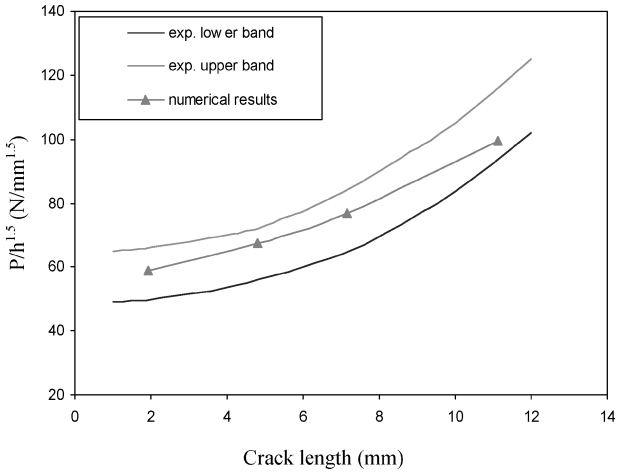

a) Test configuration 1

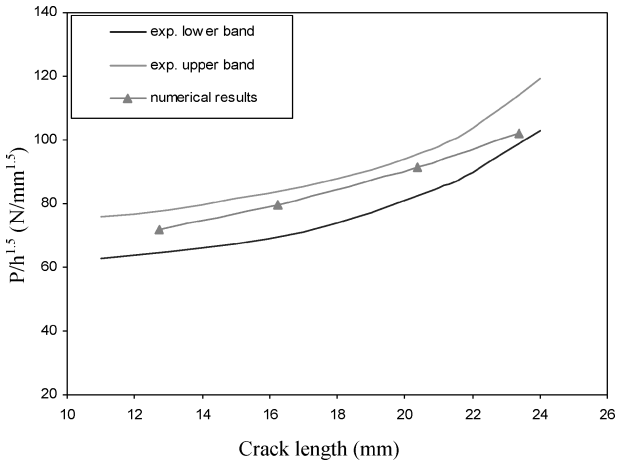

b) Test configuration 2

Fig. 3 Comparison of transverse load vs crack length relationship between calculated and experimental results.

The test results of P and those computed herein correspond to a program of loading that is "discontinuous," that is, load is applied and increased in small steps until the crack-growth criterion is satisfied (and presumably some slight crack growth occurs), and this is followed by unloading and reloading till additional crack growth occurs. Thus the values in Table 6 and plotted in Fig. 3 are the loads corresponding to incipient crack growth for a given crack length.

Influence of Variation of Model Parameters

One of the issues in the use of cohesive-layer models is the sensitivity of the predictions to small changes in model parameters, an issue that must be addressed whenever a new model is introduced in a delamination investigation. To examine this sensitivity, the model parameters, that is, h_0, $\sigma_{\max}$ (normal strength in tension), and $\tau_{\max}$ (shear strength) are varied in turn, and the values G_I and G_{II} corresponding to the two test configurations are computed for the smallest and largest crack lengths considered in each case for the same loads P given in Table 6. The results are tabulated for the four cases in Tables 7–10. The first row in all of the tables gives values based on the parameters used in the study, that is, ($h_0 = 0.02$ mm; $\sigma_{\max} = 41$ MPa; $\tau_{\max} = 97$ MPa).

From a study of the tables the following observations can be made:

1) In all four of the cases considered, an increase in the thickness from 0.020 to 0.024 mm (20% change) results in the reduction of the order of 1% in G_I and G_{II} at incipient crack growth, a change too small to make any difference from the point of view of predictions of crack growth.

2) A 10% change in $\sigma_{\max}$ (41 to 45 MPa) results in a drop of G_I by less than 1% and an increase in G_{II} by about 3% in TC-1 cases. Less significant changes are noticed in TC-2. Considering the relative largeness of G_{II_c}, the effect of a change of order of 3% in G_{II} is of little consequence.

3) A 10% increase in $\tau_{\max}$ from (97 to 107 MPa) results in a drop of G_{II} typically from 37 to 32 N/m for TC-1. Smaller changes are seen in TC-2 cases. Considering once again the largeness of G_{II_c}, the model predictions would not change in any noticeable manner.

Thus it appears the cohesive-layer model as developed here is robust and gives sufficiently consistent predictions as judged from the experimental results, at least for the relatively small changes in the model parameters considered here. Larger discrepancies caused by larger changes in the model parameters would call for an adjustment in the values of G_{I_c} and G_{II_c} for the model predictions to accord with experimental results.

Table 7 G_I and G_{II} for TC-1 at station point A ($l_{cr} = 1.92$ mm)

Properties of cohesive layer			$P/h^{1.5}$,	$p = P/2w$,	G_I,	G_{II},
h_0, mm	$\sigma_{\max}$, MPa	$\tau_{\max}$, MPa	N/mm$^{1.5}$	N/mm	N/m	N/m
0.020	41	97	58.84	2.25	204.2	36.5
0.024	41	97	58.84	2.25	202.3	36.0
0.020	45	97	58.84	2.25	202.7	37.5
0.020	41	107	58.84	2.25	204.4	31.7

Table 8 G_I and G_{II} for TC-1 at station point D ($l_{cr} = 11.12$ mm)

Properties of cohesive layer			$P/h^{1.5}$,	$p = P/2w$,	G_I,	G_{II},
h_0, mm	$\sigma_{\max}$, MPa	$\tau_{\max}$, MPa	N/mm$^{1.5}$	N/mm	N/m	N/m
0.020	41	97	99.38	3.80	203.1	37.2
0.024	41	97	99.38	3.80	201.8	37.0
0.020	45	97	99.38	3.80	202.3	38.3
0.020	41	107	99.38	3.80	203.8	32.7

Table 9 G_I and G_{II} for TC-2 at station point A ($l_{cr} = 12.72$ mm)

Properties of cohesive layer			$P/h^{1.5}$,	$p = P/w$,	G_I,	G_{II},
h_0, mm	$\sigma_{\max}$, MPa	$\tau_{\max}$, MPa	N/mm$^{1.5}$	N/mm	N/m	N/m
0.020	41	97	71.79	7.90	197.1	55.1
0.024	41	97	71.79	7.90	195.9	55.8
0.020	45	97	71.79	7.90	198.3	55.3
0.020	41	107	71.79	7.90	198.1	52.8

Table 10 G_I and G_{II} for TC-2 at station point D ($l_{cr} = 23.4$ mm)

Properties of cohesive layer			$P/h^{1.5}$,	$p = P/w$,	G_I,	G_{II},
h_0, mm	$\sigma_{\max}$, MPa	$\tau_{\max}$, MPa	N/mm$^{1.5}$	N/mm	N/m	N/m
0.020	41	97	102.24	11.25	196.3	57.0
0.024	41	97	102.24	11.25	194.2	57.0
0.020	45	97	102.24	11.25	196.7	56.9
0.020	41	107	102.24	11.25	196.5	54.0

P–l_{cr} Relationship Under Continuous Loading

Pertinent Details of the Analysis

Next, a crack-growth analysis is undertaken. With given initial crack lengths, static nonlinear analyses are conducted until significant crack growth occurs. The crack growth occurs by virtue of Eq. (2) being satisfied at the integration point of the crack-tip element at which instant the stresses are dropped to zero. The element is in effect eliminated, and the crack tip moves to the next element. Convergence difficulties were anticipated as the structure loses its equilibrium, but did not in fact materialize. Apparently the element size is sufficiently small for the Newton procedure to recapture the equilibrium with a few iterations.

Results of Continuous Crack-Growth Analysis

Nonlinear analyses were conducted with the initial crack tip at station points A, B, and C, respectively (Table 6) for the two test configurations. This time the analysis was continued until significant

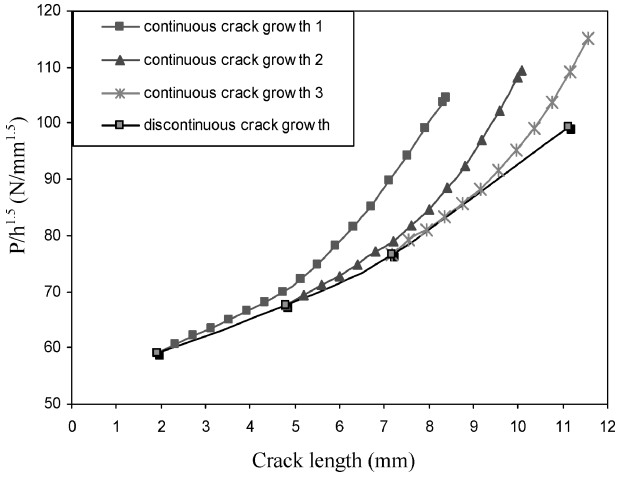

a) Test configuration 1

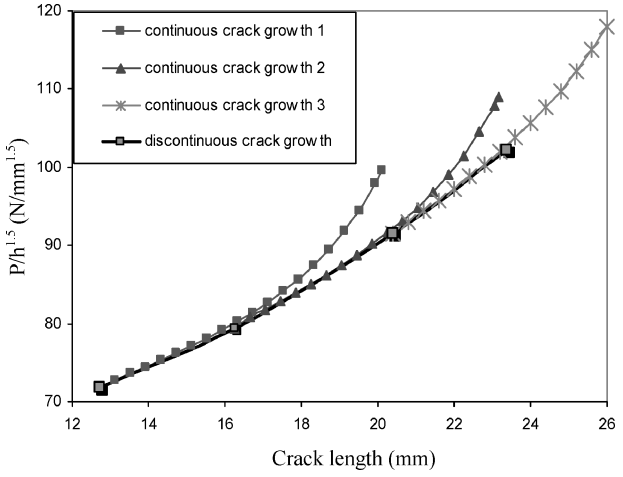

b) Test configuration 2

Fig. 4 Comparison between continuous loading program and discontinuous loading program.

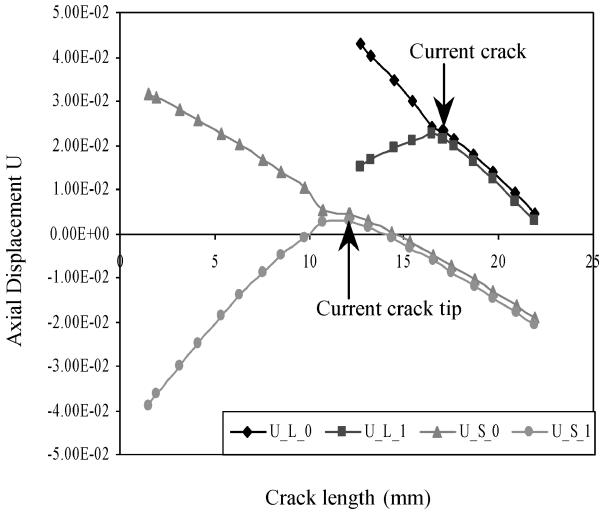

a) Vertical axis: axial displacements

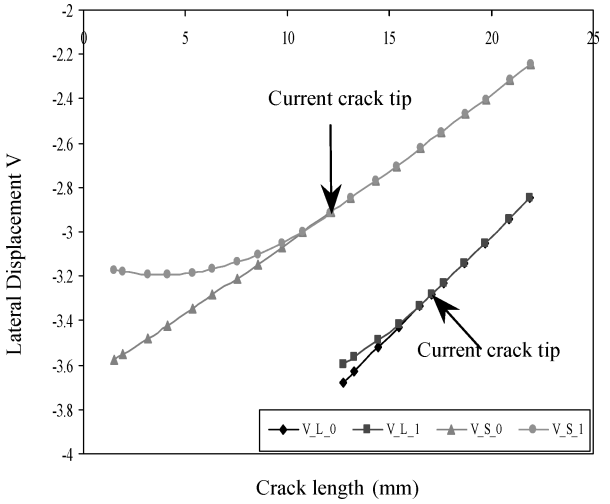

b) Vertical axis: lateral displacements

Fig. 5 Displacements along the upstream of crack under p = 8.12 N/mm for TC-2.

crack growth occurred. Typical P–l_{cr} relationships thus obtained are shown alongside the results for crack initiation (Figs. 4a and 4b). The latter corresponds to those obtained experimentally by a discontinuous loading program of loading unloading reloading discussed earlier. Note that in this case there is no actual crack growth; only the P corresponding to crack initiation are determined for various crack lengths, that is, in the analysis crack length remains fixed until the first element in the cohesive layer fails.

As an illustration, consider the case of TC-1 with initial crack length $l_0 = 1.92$ mm (station A). The P–l_{cr} relationships are shown in Fig. 4a. Consider the situation when l_{cr} is 8.0 mm. The corresponding P is given by $P/h^{1.5} \approx 100$ ($h = 2.04$ mm). In contrast consider what happens when the initial crack length $l_0 = 7.16$ mm. The load attained when l_{cr} reaches a value of 8.0 mm is given by $P/h^{1.5} \approx 80$. It is clear that there is no unique P–l_{cr} relationship as has been tacitly assumed by Jih and Sun. Similar deviations, if less spectacular, of the P–l_{cr} relationship under continuous loading from that caused by discontinuous loading are seen for TC-2. This is shown in Fig. 4b.

The results of P obtained by continuous loading accompanied by continuous crack growth depend on the initial crack length at which the loading commenced; for a given initial crack length these gradually deviate from those obtained from the discontinuous program of loading. It is seen that in the former case there is an increased resistance to crack growth with a gradual increase in G_{II} at crack growth. Thus a given crack length can correspond to several values of load (P) depending on the initial crack length selected.

It is interesting to ponder why the two modes of loading give different P for a given crack length l_{cr}. First, it must be noted in the continuous case that certain crack length is attained, in general, after the crack grows from an initial smaller crack length, and this is in contrast to the discontinuous case, in which the same crack length is maintained until the crack-tip element fails. The deviation between the two P–l_{cr} relationships is therefore attributable to the nonlinear variation of stiffness of the structure as crack growth occurs in the former case; this compounded with geometric nonlinearities tends to steer the structure toward equilibrium states, which are markedly different from those that would be attained in analyses with crack lengths fixed.

To gain further insights into this phenomenon, the deformation patterns are examined for TC-2 type laminate with differing initial crack lengths but carrying the same load P. Figures 5a and 5b show a typical result. The figure plots the axial and lateral displacements U and V, respectively, along the top and bottom of the cohesive layer (denoted by 1 and 0, respectively, in the figure) under the same load $p = 8.12$ N/mm for two cases: with initial crack lengths of 1.48 and 12.72 mm, respectively. These are denoted, respectively, by S (case 1) and L (case 2) in Figs. 5a and 5b. In case 1, the crack grows from 1.48 to 12.14 mm as the load attains to 8.12 N/mm; in case 2, the crack has an initial crack length of 12.72 mm and increases by an additional 4.36 mm. In case 1, at the load considered, the rate of advance of crack with load was found to have slowed down considerably, whereas in case 2 it remains comparatively high; the lateral deflections are significantly higher in the latter case. Careful examination revealed differences in the deformation patterns in the

vicinity of the crack tip between the two cases. In case 1 was found to have acquired a small but definite increase (10%) in mode II contribution as reflected by the values of G_{II} at the failure of the cohesive-layer elements as the load of 8.12 N/mm is approached. This could also be inferred from the differential axial displacements shown in Fig. 5a.

An important conclusion can be drawn from the foregoing discrepancies between the continuous and discontinuous loading programs and crack growth. One can associate a load P with a crack length l_{cr} only for a given initial crack length l_0. Plots of P vs l_{cr} without regard to l_0 would result in significant scatter as is seen from the plots of Jih and Sun.[2]

Impact Loading vs Static Loading

Jih[17] gives a detailed report of an investigation of delamination growth under impact loading for the two test configurations. Because the mass of the impactor (1 kg) was greater than the mass of the laminate (typically 0.1 kg) by an order of magnitude and the contact time (typically 10 m s) was found to be many times greater than half-period of the laminate (typically 0.5 m s), it was argued that the impacts came under the category of low-velocity impact; and an analysis in which the maximum impact load was treated as quasi-statically applied was considered adequate to deal with the problem. The comparisons of numerical and analytical results presented by Jih[17] and Jih and Sun[2] do suggest that this conclusion is justified to a large degree. But the comparisons do exhibit significant scatter with numerical predictions giving appreciably higher values in some cases and lower values in others. It is therefore of interest to revisit the problem and examine what conclusions a detailed analysis employing the cohesive-layer model can yield.

Given the focus on the delamination problem under a dynamic load, the present analysis does not attempt to predict the impact load history by considering the interactive contact between the impactor and laminate. The delamination behavior of the laminate is examined under an experimentally determined form of impact load vs time relationships, in which the amplitude $P_{\max}$ performs the role of a loading parameter and can be suitably prescribed. The nondimensional forms of impact load history ($P/P_{\max}$ vs time) for the two test configurations are given in Figs. 6a and 6b. This shape is experimentally determined and is approximately sinusoidal. For a given test configuration, there is a certain duration of contact, and neither the shape nor the duration of contact is found to vary noticeably with the impact velocity or the maximum load imposed or the deformation of the specimen. Thus the only variable that determines the loading history is $P_{\max}$, the maximum load sustained by the specimen.

Dynamic Analysis for Initiation of Crack Growth

In the first phase of the analysis, the objective is limited to picking up the load P_{l_0} at which the crack growth just initiates, for given initial crack length l_0. The analysis proceeds along the following lines: First, a static analysis is performed to account for thermal stresses and strains associated with curing, as in the static delamination problem. In the next step, dynamic analysis with implicit integration available in Abaqus standard is invoked. For a given crack length, a certain $P_{\max}$ is selected. The dynamic load follows the load time history already discussed (Figs. 6a and 6b). The crack growth criterion index λ is computed at the crack tip at the end of each increment of loading throughout the analysis. If it remains below 1.0 throughout, no crack growth occurs, in which case $P_{\max}$ is increased; if it exceeds 1.0 at any time during the loading, $P_{\max}$ is decreased. The analysis is rerun thus adjusting $P_{\max}$ until a value is obtained for which λ just reaches 1.0 with just the first element at the crack-tip failing.

Typical results obtained are shown in Figs. 6a and 6b. Figure 6a gives the variation of λ with time for a crack length of 4.8 mm (station point B) and $p_{\max} = 2.4$ N/mm of TC-1. Figure 6b likewise plots of the variation of λ for a crack length of 12.72 mm (station point A of TC-2) and $p_{\max} = 7.07$ N/mm. The loads in each case are those that just fail the crack-tip element at a certain point in the loading history.

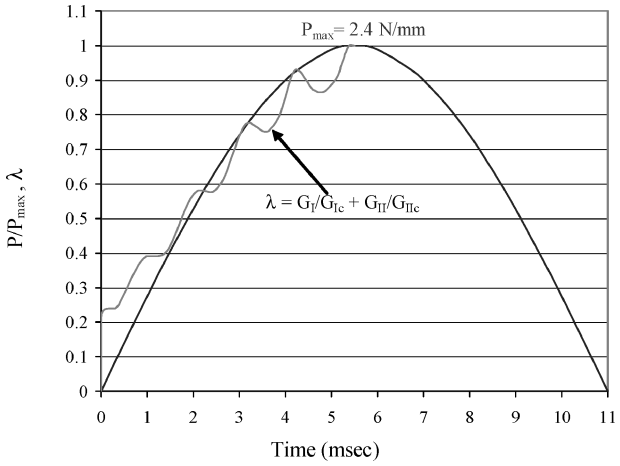

a) Test configuration 1

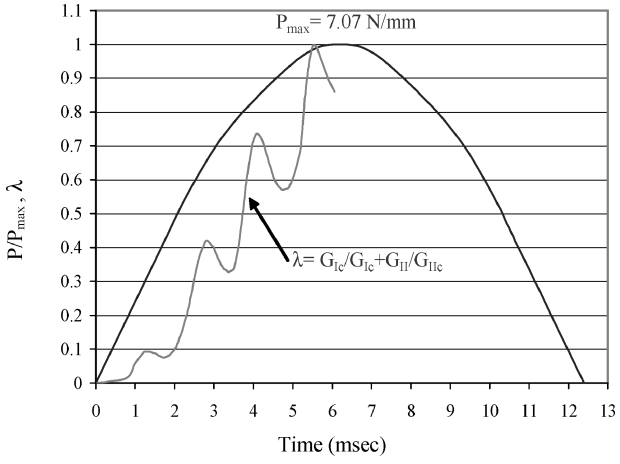

b) Test configuration 2

Fig. 6 $P/P_{\max}$ and λ vs time relationship.

The variation of λ with time in the two cases is oscillatory in nature, though increasing with load overall. This oscillation is caused, apparently by the triggering of a mode of a higher frequency localized near the crack-tip region, leading to oscillations in the crack-opening displacements. For TC-1, the value of λ has a head start, starting with a value of 0.2 at the beginning of the loading caused by curing stresses and strains. This effect is not significant for TC-2.

In general, loads at which crack-growth initiation occurs under dynamic loading are smaller than the corresponding loads for static loading. This is because of the oscillatory nature of λ, which shoots to a value of unity at the crest of an oscillation causing the crack-tip element to fail. The differences in the static and dynamic values of P_{l_0} are not large but significant from the point of view of engineering predictions. For example, for TC-1, with $l_0 = 4.8$ mm, the static and dynamic values of P_{l_0} are 2.58 and 2.40 N/mm, respectively; for TC-2, with $l_0 = 12.72$ mm, they are, respectively, 7.90 and 7.07 N/mm.

Jih[17] has given plots of load amplitude vs impact velocity relationships for the two test configurations, and in the range of interest ($0.6\,\text{m/s} < v < 1.8\,\text{m/s}$) the plots can be represented by the following linear relationships:

1) For TC-1,

$$P_{\max}/h^{1.5} = 5 + 94v \tag{3}$$

2) For TC-2,

$$P_{\max}/h^{1.5} = 25 + 40.333v \tag{4}$$

where h is the overall thickness of the laminate (2.04 and 2.6 mm for TC-1 and TC-2, respectively) and v is the impact velocity in m/s.

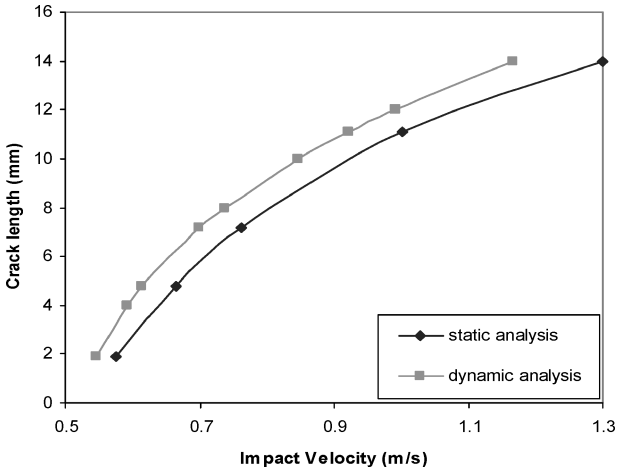

a) Test configuration 1

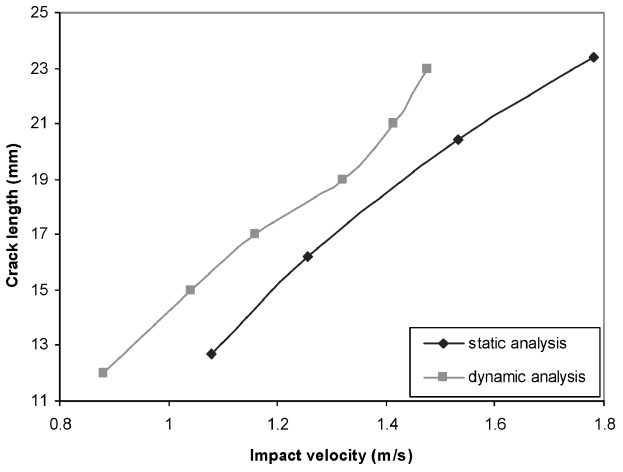

b) Test configuration 2

Fig. 7 The v–l_0 relationship under dynamic loading and static loading.

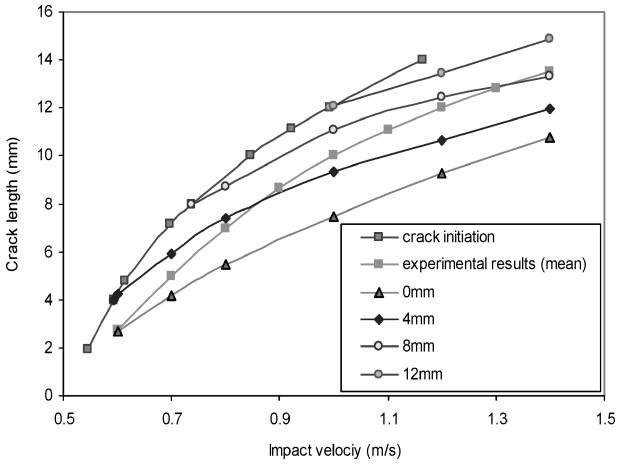

a) Test configuration 1

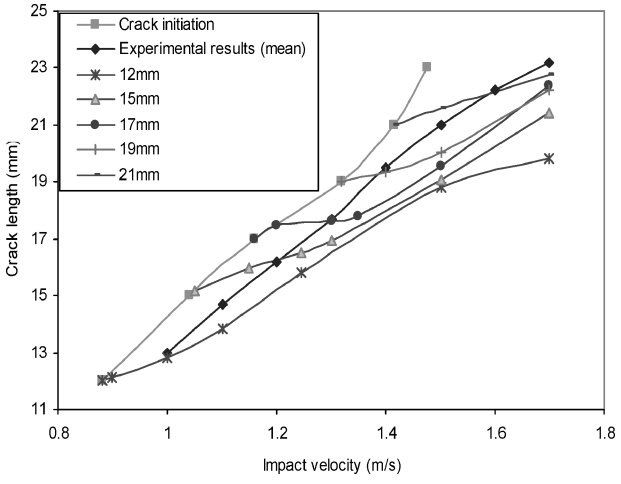

b) Test configuration 2

Fig. 8 The v–l_{max} relationship.

Thus it is possible plot the relationship between impact velocity and crack length for the two cases. These plots are shown in Figs. 7a and 7b. To compare these results with those under static loading, fictitious impact velocities are obtained by substituting the values of quasi-statically applied P corresponding to crack initiation in the foregoing equations and evaluating the v. These results of v thus obtained are plotted against $l_{cr}(=l_0)$ in the same figure. It is seen that the crack lengths in the static case are smaller than those of dynamic loading for any given v.

Crack Growth Under Dynamic Loading

To examine the crack growth under dynamic loading, a certain crack length l_0 is selected, and the impact velocity (i.e., P_{max}) is increased in steps to obtain the maximum crack length attained in each case l_{max}. Thus a relationship between the l_{max} and impact velocity v is developed. Such relationships are obtained for various values of l_0 for both TC-1 and TC-2. These are shown in Figs. 8a and 8b, respectively, with the corresponding l_0 indicated in the index. Plotted also in these figures are 1) the relationship between the l_0 and v corresponding to crack initiation and 2) the averaged values of l_{max} for various impact velocities as determined experimentally.[2]

The two figures appear different in details but exhibit some common features:

1) For a given P_{max} (or v) in the P_{max} vs l_{cr} relationship, the maximum value of $l_{cr} = l_0$, which is found along the crack initiation line. The l_{cr} vs v relationship for any given l_0 takes off from this characteristic at the point where $l_{cr} = l_0$.

2) These characteristics tend to be much flatter than that corresponding to crack initiation.

3) Those with the smaller l_0 tend to lie below those with a higher l_0, indicating the role played by the initial crack length. The maximum crack length attained for any given impact velocity or P_{max} increases with the initial crack length l_0.

4) Together, all of these characteristics cover a patch of area on either side of the mean l_{cr} vs v relationship obtained from experiments of Jih and Sun.[2] This explains the scatter observed in the experimental plots where no consideration has been given to l_0 as a parameter. In the experiments the same specimen is used repeatedly to obtain the maximum crack length attained as a function of impact velocity. Obviously the impact velocity increases with successive impacts as also l_0, the initial crack length. This gives rise to a relatively steep increase of l_{max} with impact velocity, so much so the mean experimental characteristic follows the same trend as the crack initiation characteristic. Therefore, a single blow with a given impact velocity causes less delamination than a sequence of impacts with gradually increasing impact velocity leading up to the given value.

Even though the initial crack length appears to be a factor in the rate of crack growth, more work needs to be done to establish this conclusion on empirical and rational bases. Introduction of a finite layer of cohesive material can itself have a strong local influence as to steer the computed response away from reality. The authors are currently seeking more experimental evidence to examine this aspect of the problem.

Conclusions

The following conclusions can be drawn from this study:

1) The cohesive-layer technique can perform a dual role of identifying the critical values of strain-energy release rate and tracing

delamination growth. The critical values of SERR thus determined are relative values only and must be used only in conjunction with the model used to determine them.

2) The model as developed here is based on an element in which the stresses corotational with the element and incremental strains are computed using an updated set of local axes and the current dimensions of the element. Thus large rotations are handled effectively in the computation of the cohesive-layer response. This model is proved to be fairly robust because 10% change in the values of maximum stresses or 20% change in the thickness do not produce any significant difference in predicted loads for crack initiation.

3) The relationship between the impact load and crack length attained is found to be a function of the initial crack length.

4) The crack growth under dynamic loading is greater than that for a quasi-statically applied load for a given impact load. This is found to be the result of local vibrations, which cause oscillations of the crack-opening displacements and have a much higher frequency than the overall frequency of the entire beam. The phase of vibration associated with an increased crack opening coincides with the phase of rapid crack growth.

5) The scatter in the experimental results of Jih and Sun[2] can be satisfactorily explained by tracing the crack growth with a spectrum of initial crack lengths.

Acknowledgments

The work reported here was supported in part by a Boeing Fellowship grant offered by the Boeing Foundation, St. Louis. Mark J. Johnson acted as the Boeing Contact.

References

[1]Abrate, S., "Impact Dynamics," *Impact on Composite Structures*, Cambridge Univ. Press, New York, 1998, pp. 26–134.

[2]Jih, C. J., and Sun, C. T., "Prediction of Delamination in Composite Laminates Subjected to Low Velocity Impact," *Journal of Composite Materials*, Vol. 27, No. 7, 1993, pp. 684–701.

[3]Barrenblatt, G. I., "The Mathematical Theory of Equilibrium Cracks in Brittle Fracture," *Advances in Applied Mechanics*, Vol. 7, 1962, pp. 55–129.

[4]Dugdale, D. S., "Yielding of Sheets Containing Slits," *Journal of Mechanics and Physics of Solids*, Vol. 8, 1960, pp. 100–104.

[5]Williams, M. L., "The Fracture of Visco-Elastic Material," *Fracture of Solids*, edited by G. Drucker, Interscience Publishers, New York, 1963, pp. 157–188.

[6]Schapery, R. A., "A Theory of Crack Initiation and Growth in Visco-Elastic Media," *International Journal of Fracture*, Vol. 11, No. 1, 1975, pp. 141–159.

[7]Ungsuwarungsri, T., and Knauss, W. G., "The Role of Damage-Softened Material Behavior in the Fracture of Composites and Adhesives," *International Journal of Fracture*, Vol. 35, No. 3, 1987, pp. 221–241.

[8]Needleman, A., "A Continuum Model for Void Nucleation by Inclusion Debonding," *Journal of Applied Mechanics*, Vol. 54, No. 3, 1987, pp. 525–531.

[9]Needleman, A., "An Analysis of Decohesion Along an Imperfect Interface," *International Journal of Fracture*, Vol. 42, No. 1, 1990, pp. 21–40.

[10]Shahwan, K. W., and Waas, A. M., "Non-Self-Similar Decohesion Along a Finite Interface of Unilaterally Constrained Delaminations," *Proceedings of the Royal Society of London*, Vol. 453, March 1997, pp. 515–550.

[11]Song, S. J., and Waas, A. M., "Energy-Based Mechanical Model for Mixed Mode Failure of Laminated Composites," *AIAA Journal*, Vol. 33, No. 4, 1995, pp. 739–745.

[12]Rahulkumar, P., Jagota, A., Bennison, S. J., and Saigal, S., "Cohesive Element Modeling of Viscoelastic Fracture: Application to Peel Testing of Polymers," *International Journal of Solids and Structures*, Vol. 37, No. 13, 2000, pp. 1873–1897.

[13]El-Sayed, S., and Sridharan, S., "Performance of a Cohesive Layer Model in the Prediction of Interfacial Crack Growth in Sandwich Beams," *Journal of Sandwich Structures and Materials*, Vol. 4, Jan. 2002, pp. 31–48.

[14]El-Sayed, S., and Sridharan, S., "Cohesive Layer Models for Predicting Delamination Growth and Crack Kinking in Sandwich Structures," *International Journal of Fracture*, Vol. 117, No. 1, 2002, pp. 63–84.

[15]Alfano, G., and Crisfield, M. A., "Finite Element Interface Models for the Delamination Analysis of Laminated Composites: Mechanical and Computational Issues," *International Journal of Numerical Methods in Engineering*, Vol. 50, Jan. 2001, pp. 1701–1736.

[16]Blackman, B. R. K., Handavinia, H., Kinloch, A. J., and Williams, J. G., "The Use of a Cohesive Zone Model to Study the Fracture of Fibre Composites and Adhesively-Bonded Joints," *International Journal of Fracture*, Vol. 119, No. 1, 2003, pp. 25–46.

[17]Jih, C. J., "Analysis of Delamination in Composite Laminates Under Low Velocity Impact," Ph.D. Dissertation, School of Aeronautics and Astronautics, Purdue Univ., West Lafayette, IN, Dec. 1991.

[18]Charalambides, M., Kinloch, A. J., Wang, Y., and Williams, J. G., "On the Analysis of Mixed-Mode Failure," *International Journal of Fracture*, Vol. 54, No. 3, 1992, pp. 269–291.

[19]Vinson, J. R., and Sierakowski, R. L., *The Behavior of Structures Composed of Composite Materials*, Martinus Nijhoff, Dordrecht, The Netherlands, 1986, p. 60.

[20]"User Subroutine to Define a Material's Mechanical Behavior," *ABAQUS/Standard/Users's Manual*, Ver. 6.3, Hibbitt, Karlsson and Sorensen, Inc., Pawtucket, RI, 2001, pp. 24.2.30.1–24.2.30.14.

[21]"Rate of Deformation and Strain Increment," *ABAQUS/Theory Manual*, Ver. 5.5, Hibbitt, Karlsson and Sorensen, Inc., Pawtucket, RI, 1995, pp. 1.4.3.1–1.4.3.4.

K. Shivakumar
Associate Editor